Journal of Membrane Science 668 (2023) 121215

Contents lists available at ScienceDirect

Journal of Membrane Science

journal homepage: www.elsevier.com/locate/memsci

Cyclomatrix polyphosphazene organic solvent nanofiltration membranes

Farzaneh Radmanesh [a], Gerrald Bargeman [a,b], Nieck E. Benes [a,*]

[a] Membrane Science and Technology Cluster, Faculty of Science and Technology, MESA+ Institute for Nanotechnology, University of Twente, P.O. Box 217, 7500 AE, Enschede, the Netherlands

[b] Research and Development Group, Nobian Industrial Chemicals B.V., Zutphenseweg 10, P.O. Box 10, 7400 AA, Deventer, the Netherlands

ARTICLE INFO

Keywords:
Interfacial polymerization
polyphosphazene
organic solvent
nanofiltration

ABSTRACT

In this work, we report the synthesis and characteristics of cyclomatrix polyphosphazene membranes based on interfacial polymerization between 1,1-tris(4-hydroxyphenyl)ethane and hexachlorocyclotriphosphazene on top of alumina or polyacrylonitrile supports. The potential of alumina-supported thin film composite membranes as organic solvent nanofiltration membranes has been confirmed with a polystyrene-based molecular weight cutoff of 347 ± 120 Da and 503 ± 220 Da in acetone and toluene, respectively. Also, the resulting alumina-supported TFC membrane showed a methylene blue rejection (M_w = 319 g mol^{-1}) of 98.2 ± 2.3%, 92 ± 1.7%, and 93 ± 0.5% in water, ethanol, and acetone, respectively. Furthermore, a thin film composite membrane has been prepared with a polyacrylonitrile support via interfacial polymerization to validate the preparation technique for polymeric supports and facilitate industrial implementation. The resulting membrane showed higher permeance and lower rejection than the alumina-supported membrane due to the presence of pinholes in the selective layer on top of the polyacrylonitrile supports. Our results clearly show the great potential of cyclomatrix polyphosphazene membranes as organic solvent nanofiltration membranes. However, for polyacrylonitrile-supported membranes, the preparation method needs further investigation.

1. Introduction

Nanofiltration (NF) is a pressure-driven technology that plays an indispensable role in separation processes in the industry, including water softening, food processing, and purification of primary materials and solvents [1–5]. With pore diameters of 0.5–2 nm, NF membranes are suitable for removing small organic molecules such as micropollutants and multivalent ions from liquids or separating multivalent ions from monovalent ions, even at high concentrations [6–8]. A particular category of NF membranes that can resist and perform the separation in organic solvents is organic solvent nanofiltration (OSN). To allow for this type of separation, the membrane material must be stable in organic solvents to guarantee its stable performance. In recent years, there has been considerable interest in developing thin film composite membranes (TFC) suitable for OSN via interfacial polymerization (IP). The focus of those studies is to augment the membrane permeability, selectivity, and solvent stability via structural and pore design [9–18]. Numerous methods have been deployed to this aim, such as altering monomers and supports and tuning the cross-linking degree [9–15]. To date, conventional IP procedures for various types of polymers, such as polyamide, polyimide, polyester, covalent organic framework (COF), and covalent organic polymer (COP), have been explored [13,19,20].

Polyphosphazene (PPz) is a class of inorganic-organic hybrid polymers known for its robustness, flexibility in its structural design, and tunability of its properties [21]. It comprises a backbone of alternating nitrogen and phosphorous atoms accompanied by two organic substituents linked to each phosphorous atom [22]. The two main monomers for preparing PPz are hexachlorocyclotriphosphazene (HCCP) and poly(dichlorophosphazene) (PDCP). The chlorine group present in these monomers can easily be substituted via nucleophilic attack by various monomers containing amino or hydroxyl groups [23]. Different PPz architectures have been synthesized, including linear, star-shaped, dendritic, cyclolinear, and cyclomatrix polyphosphazene (CPPz) structures [24]. Accordingly, different kinds of PPz with distinct properties have been designed on a molecular scale. Among those architects, cyclomatrix polyphosphazene is known for its superior chemical stability and solvent resistance [25].

To the best of our knowledge, only a limited number of studies have investigated the use of polyphosphazene-based materials as nanofiltration membranes, and only for application in aqueous environments

* Corresponding author. Membrane Science and Technology Cluster, Faculty of Science and Technology, MESA+ Institute for Nanotechnology, University of Twente, P.O. Box 217, 7500 AE, Enschede, the Netherlands.

E-mail address: n.e.benes@utwente.nl (N.E. Benes).

https://doi.org/10.1016/j.memsci.2022.121215
Received 29 September 2022; Received in revised form 16 November 2022; Accepted 21 November 2022
Available online 23 November 2022
0376-7388/© 2022 The Authors. Published by Elsevier B.V. This is an open access article under the CC BY license (http://creativecommons.org/licenses/by/4.0/).

[26,27]. You et al. [26] prepared a positively charged polyamine-based CPPz NF membrane via IP of polyethyleneimine (PEI) and HCCP. They showed that their produced membrane has a water permeance of 3.7 L m^{-2} h^{-1} bar^{-1} and a rejection of up to 97% for $MgCl_2$ and 82% for methylene blue (a chloride salt of a cationic dye with Mw = 319.85 g mol^{-1}). Allen et al. [27] focused on fabricating linear poly(bis(phenoxy) phosphazene) membranes on a porous support and studied the diffusion of Cr^{3+}, Co^{2+}, and Mn^{2+} through the membrane. Both studies indicated the technical feasibility of PPz based membranes as NF membranes for aqueous applications. Since these authors only reported the solute rejection in water, to date, there has not been a detailed investigation on the potential of CPPz membranes for OSN applications.

Obtaining a good rejection for small molecules with a $M_w < 400$ g mol^{-1} in combination with an acceptable permeance is always challenging for OSN membranes, when they are prepared with IP. To this aim, the membrane should have small and precise well-distributed pores, which often leads to a relatively low solvent flux as a consequence of the often encountered trade-off between selectivity and permeance [1]. To the best of our knowledge, limited studies, such as [10,13,28–38], succeeded in developing membranes with a rejection above 90% for dyes with M_w of 314 g mol^{-1} to 328 g mol^{-1} and acceptable ethanol permeances of more than 1 L m^{-2} h^{-1} bar^{-1}.

The goal of this work is to prepare CPPz OSN membranes via IP, with properties that make them suitable for rejecting small solutes with a $M_w < 500$ g mol^{-1} in various solvents. To achieve this goal, we consider a recently developed one-step IP method, suitable for preparing ultrathin cyclomatrix poly(phenoxy)phosphazene hybrid membranes for gas separation [39], to be a promising preparation method for OSN membranes as well. In this method, a thin film poly(phenoxy)phosphazene network is formed via a polycondensation reaction on top of the ceramic support. For gas separation membranes, first, a biphenol or a tri/dihydroxybenzene is dissolved in a DMSO/KOH solution to convert the hydroxyl groups to anions that are crucial for the reaction to proceed [39,40]. In the second step, the formed phenolates react with HCCP in cyclohexane during a nucleophilic substitution reaction in which HCl is eliminated, and a highly cross-linked structure of CPPz is formed. The goal of the current contribution is to demonstrate that selecting larger organic bridges and reducing the extent of cross-linking results in CPPz membranes with NF properties suitable for OSN applications. We hypothesize that the length, flexibility, and reactivity of the phenolates directly affect the chain's mobility, pore size, and distribution. Provided that our hypothesis holds, which we intend to show in this manuscript, the facile nature of the technique used for membrane synthesis allows for tuning the properties of the membrane and changing its applicability from gas separation to nanofiltration.

Furthermore, to the best of our knowledge, it is the first time that it has been tried to prepare CPPz membranes by combining HCCP and 1,1-Tris(4 hydroxyphenyl)ethane (TPE) and use these membranes for OSN application. The membranes have been prepared through IP between TPE and HCCP, creating a thin film composite layer on an alumina or a PAN support. The CPPz TPE-HCCP network has been characterized, and the performance of the prepared membrane has been evaluated in detail with different solvents, including toluene, ethanol, and acetone. The experimental work presented here provides one of the first investigations into the feasibility of implementing CPPz-based nanofiltration membranes in OSN applications.

2. Experimental

2.1. Materials

1,1-Tris(4 hydroxyphenyl)ethane (TPE, >98.0%) was purchased from TCI (Belgium). Phosphonitrilic chloride trimer (HCCP, 99%), dimethyl sulfoxide (DMSO, anhydrous, ≥99.9%), tetrahydrofuran (THF, ≥99%), *N,N*-Dimethylformamide (DMF, 99.8%), Methylene Blue (MB, 97%), sodium chloride (NaCl, ≥99%), and poly(ethylene glycol) (PEG) with molecular weights of 400, 600, and 1500 g mol^{-1} were obtained from Sigma-Aldrich (The Netherlands). A 1 L bottle of dihydrolevoglucosenone, or Cyrene (99.3%), was supplied by the Circa Group. Brilliant Yellow (BY, 70%) was purchased from Aldrich. Cyclohexane (EMSURE for analysis), sodium sulfate (Na_2SO_4, anhydrous, for analysis EMSURE ACS), magnesium sulfate heptahydrate ($MgSO_4$, for analysis EMSURE ACS), PEG 1000 (EMPROVE ESSENTIAL), Rhodamine B (RB) and potassium hydroxide (KOH, pellets extra pure) were acquired from Merck kGaA. Ethanol (EtOH, technical grade) was purchased from Boom. Magnesium chloride hexahydrate ($MgCl_2{\cdot}6H_2O$, 99.0–100.0%, AnalaR NORMAPUR ACS Reag.) was obtained from VWR chemicals (Netherlands). PEG 200 was obtained from Fluka (Germany). All chemicals were used as received.

α-alumina discs (39 mm of diameter, 2 mm of thickness, and pore size of 80 nm) with one polished side were obtained from Pervatech B·V, the Netherlands, and used as supports. A 3 μm γ-alumina layer was fabricated on the polished surface of the α-alumina according to earlier reports [41]. Depending on the procedure, the formed γ-alumina layer typically has a pore diameter between 3 and 8 nm serving as an intermediate layer for preparing the selective polymeric layer (Fig. S1), [42]. Porous polyacrylonitrile (PAN) ultrafiltration supports, UF010104, with a molecular weight cutoff of 10 kDa, were obtained from Solsep, the Netherlands [43,44].

2.2. Material fabrication

Both TPE-HCCP free-standing films and membranes on inorganic or polymeric supports were prepared by conducting interfacial polymerization (IP) between 10 w/v% TPE in DMSO (hydroxyl molar ratio of TPE:KOH of 0.85) and 3.5 wt% HCCP in cyclohexane. First, KOH with the mentioned hydroxyl molar ratio of TPE to KOH was added to a 10 wt % TPE solution in DMSO and heated for 2.5 h at 80 °C. Subsequently, it was brought into contact with the HCCP solution according to the procedures described below.

2.2.1. Synthesis of TPE-HCCP free-standing films

The TPE-HCCP free-standing layer was prepared in the following way. A 3.5 wt% HCCP solution in cyclohexane was gently poured atop the TPE solution to minimize disturbances of the top layer of the TPE solution. A thin layer formed at the interface of the two phases as the two solutions contacted. After 30 min, the free-standing films were collected with a tweezer, filtered, and washed 3 times with ethanol, acetone, and water. Then, the solid films were dried in a vacuum oven at 50 °C.

2.2.2. Preparation of alumina-supported TPE-HCCP TFC membranes

TFC membranes were prepared by IP atop the ceramic support using an IP cell reported earlier [45]. The support and IP set-up were warmed up in a closed box located in an oven at 80 °C for 30 min. After this, 5 mL of TPE solution was poured on top of the support, and it was placed in the oven at 80 °C for 15 min. Subsequently, the cell was taken from the oven, and the remaining TPE solution on top of the support was discarded. After that, the surface of the support was dried from the remaining TPE solution droplets using a rubber roller and N_2 gun. Then the HCCP solution was poured on top of the support slowly. After 15 min of reaction at room temperature, the HCCP solution was discarded, and the membrane surface was rinsed three times with ethanol. It was dried overnight in a fume hood and then kept in the vacuum oven at 50 °C before further analysis.

2.2.3. Preparation of PAN-supported TPE-HCCP thin-film composite membranes

PAN-supported TPE-HCCP thin-film composite membranes were fabricated as follows. A 7 cm × 10.5 cm piece of the PAN support was soaked in water overnight to wet the pores and remove any residuals. Subsequently, the water droplets on the support's surface were dried, and the support was placed in an IP cell reported earlier [46]. Then, 25

mL of the TPE solution was poured on top of the support membrane and left to soak for 10 min at room temperature. Subsequently, the remaining TPE solution was discarded, and the surface of the support was dried with an N_2 gun and paper tissue to obtain a dry surface. Next, 25 mL HCCP solution was poured on top of the support, and it was left to react for 10 min at room temperature. The remaining solution was removed, and the membranes were rinsed with ethanol. The membrane's surface was dried in a fume hood for 5 min, followed by thermal treatment of the membrane at 65 °C for 5 min. After this temperature treatment it was stored in Milli-Q water before characterization. It is worth mentioning that the thermal treatment was added to improve membrane rejection.

2.3. Physical and chemical characterization

The membrane characterization was done according to the procedure previously reported [47]. Field-emission scanning electron microscopy (FE-SEM) images were obtained with Zeiss MERLIN high-resolution scanning electron microscope using an accelerating voltage of 1.4 kV to visualize the thickness and morphology of the membranes. For the sample preparation, membranes were dried overnight in a vacuum oven at 50 °C and fractured in liquid nitrogen. EDX analysis was performed at 10 kV with >1000 counts/s on the spouter-coated 5 nm Pt/Pd samples. Fourier transform infrared spectroscopy (FTIR) measurement was done on the free-standing film using a PerkinElmer UATR Spectrum Two to examine the chemistry of the free-standing film. The dried free-standing film was scanned between the wave numbers of 4000 to 550 cm^{-1} in reflectance mode at a resolution of 4 cm^{-1} for a minimum of 32 scans. X-Ray Fluorescence (XRF) measurements (S8 Tiger, Bruker) were performed on the free-standing films. Cyclohexane permporometry was used to determine the pore diameter of the support and the prepared membrane using the procedure reported earlier [48]. The zeta potential measurements were performed as reported earlier [49], with an electrokinetic analyzer SurPASS system (Anton Paar, Graz Austria) and a 0.005 M KCl solution.

2.4. Chemical stability characterization

To determine the potential of the networks as a membrane for OSN applications, the free-standing films were kept in THF, Cyrene, DMF, and DMSO for 30 h and the free-standing films were visually checked at the start and after 30 h.

2.5. Membrane performance characterization

Permeance and dye rejection data were collected using Sterlitech stainless steel cells (model HP4750) with a pressure of 5–21 bars. Pure solvent permeance data were determined by weighing the permeate sampled, m (g), during timed intervals using four applied transmembrane pressures between 8 and 21 bar and taking the slope of a linear fit of the collected pressure – flux data forced through the origin. The solvent permeance was calculated using Equation (1):

$$P = \frac{m}{\rho \times A \times t \times \Delta p} \tag{1}$$

where ρ (g L^{-1}) is the density of the pure solvent obtained from the manufacturer, A (m^2) is the effective membrane filtration area, t (h) is the liquid sampling time, and Δp (bar) is the applied transmembrane pressure.

Dyes rejection measurements were conducted using single dye solutions of BY (a divalent anionic sodium salt with $M_w = 624.55$ g mol^{-1}, 50 ppm), RB (a monovalent cation chloride salt $M_w = 479.02$ g mol^{-1}, 50 ppm), and Methylene Blue (MB, a monovalent cation chloride salt with $M_w = 319.85$ g mol^{-1}, 50 ppm) in either water, ethanol or acetone. The rejection was calculated using Equation (2)

$$R = 1 - \frac{C_p}{\frac{(C_R + C_F)}{2}} \tag{2}$$

where R, C_p, C_F and C_R are the rejection, permeate concentration, feed concentration and retentate concentration. The retentate and permeate samples were obtained at a recovery between 45% and 70%. Between each measurement, the membranes were washed in acetone and ethanol several times, at least for 24 h. Solute concentrations of BY, RB, and MB were calculated from PerkinElmer λ12 UV–Vis spectrophotometer results at the characteristic wavelengths of 401.3 nm (BY/water), 554.4 nm (RB/water), 664.8 nm (MB/water), 655 nm (MB/ethanol), 552.9 nm (RB/ethanol), 657 nm (MB/acetone), and 556.2 nm (RB/acetone). The dye adsorption during the rejection measurement was calculated as follows:

$$M_{ads} = M_f - M_R - M_p \tag{3}$$

where M_{ads}, M_f, M_R and M_p are the mass of dyes adsorbed on the membrane and in the feed, retentate, and total permeate, respectively. The adsorbed dye percentages were calculated to be between 0.2% and 4%. Also, to eliminate the dye adsorption on the ceramic support during rejection measurements, for some measurements, the set-up was filled one more time after reaching the mentioned recoveries for the first run, and the test was repeated.

Salt rejection measurements for both types of membranes were performed in batch mode in a custom-built set-up with an effective membrane area of 7.548 cm^2, as reported earlier [46]. The membrane was placed at the bottom of a stainless steel vessel. The vessel was filled with 1 L of salt solution and pressurized to 10 bar with nitrogen gas. During the measurement, the solution was stirred with an overhead stirrer at 500 rpm to minimize concentration polarization. The salt rejection was assessed with 2 g L^{-1} aqueous single salt solutions of $MgSO_4$, $MgCl_2$, Na_2SO_4, or NaCl. After collecting 10 mL of permeate, the samples were collected from permeate and retentate directly from the cell. The salt rejection was calculated using Equation (2). The salt concentration was derived using a 3310 conductivity meter (WTW, Germany).

PEG molecular weight cutoff (MWCO) for both types of membranes was measured using an aqueous solution of PEGs mixtures and the same set-up used for salt rejection. For this purpose, PEGs with mean molecular weights of 200, 400, 600, 1000, and 1500 g mol^{-1} were used, each at a concentration of 1 g L^{-1}. After collecting 10 mL of permeate, the samples were collected from permeate and retentate directly from the cell. The PEG concentrations in the feed, the permeate, and the retentate were assessed using gel permeation chromatography (GPC, Agilent Technologies 1200/1260 Infinity GPC/SEC series) according to a previously described protocol [50]. The PEG rejection was then calculated using Equation (2) and the MWCO was determined as the molar mass that is retained for 90%. The polystyrene-based MWCO was determined with 0.5 g L^{-1} and 1 g L^{-1} synthesized polystyrene of broad molecular weight between 200 and 1500 g mol^{-1} in acetone and toluene, respectively and the earlier described procedure was followed to calculate the polystyrene-based MWCO.

In addition, the PEG-based MWCO data can be used to determine the pore diameter of the selective layer [51,52]. PEG molecules can form spheres of a certain radius in the solution, and their molecular weight, M_w (g mol^{-1}), can be related to the PEG radius and diameter, r (Å) and d (Å), via the Stokes-Einstein equation [53]:

$$r = 0.1673\, M_w^{0.557} \tag{4}$$

$$\text{with } d = 2r \tag{5}$$

Equations (4) and (5) can be used to determine μ_p and σ_p, the mean effective pore diameter based on the solute radius obtained for a rejection of $R = 50\%$ and the geometric standard deviation, defined as the

ratio between the values of the pore diameter at $R = 84.13\%$ and $R = 50\%$, respectively.

Two models have been proposed in literature to calculate the pore size distribution. In the first model, the influence of hydrodynamic and steric interactions between solutes and pore sizes on solute rejection is neglected and the pore diameter is assumed to be equal to the solute diameter ($d_p = d$). The mean pore diameter μ_p in this case can be determined directly from equations (4) and (5) by substituting the PEG molecular weight for which a rejection of $R = 50\%$ is obtained in equation (4).

In the second model, the steric and hydrodynamic hindrances between solutes and pore sizes on solute rejection are taken into consideration and the relation between the pore diameter and the PEG solute diameter for which $R = 50\%$ is obtained can be expressed as [54]:

$$\mu_p = \frac{d_{R=50\%}}{0.416} \tag{6}$$

where the PEG diameter at $R = 50\%$, $d_{R=50\%}$, is obtained from the PEG molecular weight for which a rejection of $R = 50\%$ is obtained and equations (4) and (5).

After substituting μ_p and σ_p in Equation (7) and solving this equation, the probability density function and the pore size distribution of the membrane are obtained [55].

$$\frac{dR(d_p)}{dd_p} = \frac{1}{d_p \ln \sigma_p \sqrt{2\pi}} \exp\left[-\frac{(\ln d_p - \ln \mu_p)^2}{2(\ln \sigma_p)^2}\right] \tag{7}$$

Where d_p is the pore diameter.

It should be noted that this pore size distribution function has originally been determined for ultrafiltration membranes, but it has been applied for NF membranes regularly as well and its applicability has recently been re-evaluated [54].

3. Results and discussion

The results and discussion section is split up into three parts. In the first part, we will discuss the formation and characterization of the TPE-HCCP free-standing films. The second part will focus on the characterization and performance of the alumina-based membrane featuring the solvent permeances and the solute rejections. Finally, in the third part, we will evaluate the formation and performance of PAN-based TPE-HCCP membranes.

3.1. Formation and characterization of the polyphosphazene free-standing film

Interfacial polymerization between TPE in DMSO and HCCP in cyclohexane results in the formation of a cyclomatrix polyphosphazene TPE-HCCP layer at the interface of the two solutions, as shown in Fig. 1A. Before the reaction, TPE is deprotonated by KOH, forming readily reactive anions which participate in the nucleophilic substitution of chlorine attached to the triazatriphosphorine ring [39]. One should note that the use of DMSO as solvent is necessary to enhance the nucleophilicity of TPE and, subsequently, to establish the network. At the DMSO-cyclohexane interface, the phenolates react with HCCP to form the cyclomatrix polyphosphazene network, as shown in Fig. 1B.

FTIR is used to evaluate the chemistry of the formed networks. Fig. 2 shows the FTIR spectrum of the used monomers and prepared networks. The TPE-HCCP network demonstrates the characteristic peaks of both monomers, TPE and HCCP, as well as the new peaks of the formed bonds during the IP reaction. The network reveals two peaks around 1499 cm^{-1} and 1599 cm^{-1} belonging to the C═C stretching vibrations of the aromatic ring of the TPE monomers. Also, the weak band at 2970 cm^{-1} originates from the asymmetric stretching mode of the sp^3 C–H bond in the CH_3 group [56,57]. The HCCP is apparent from the broad peak at 1100–1200 cm^{-1}, ascribed to the asymmetric P═N–P stretching, and a peak at 875 cm^{-1} related to the symmetric P═N–P stretching [58,59]. The P–Cl bond with peaks at 595 cm^{-1} and 511 cm^{-1} has disappeared to some extent [60]. Finally, a new peak appearing at 940 cm^{-1} can be assigned to the formation of P–O-Ar bonds [61]. In summary, we can confirm the formation of the TPE-HCCP network with FTIR.

Table 1 summarizes the result of all the methods used for elemental analysis of the TPE-HCCP free-standing layer. The results from all the methods are in good agreement and show that the number of reacted Cl is between 2 and 3 per HCCP. The number of reacted Cl was calculated based on the ratio of C/N, P/C, and P/Cl. Though the possibility of Cl hydrolysis in the presence of water and formation of KCl as by-product is high, the calculated reacted Cl based on the ratio of P/Cl, still matches well with other methods calculated based on C/N and P/C ratios. We conclude that the hydrolysis of Cl during preparation is negligible.

Preliminary chemical stability experiments on TPE-HCCP free-standing films showed that the polymer networks do not dissolve in solvents such as THF, Cyrene, DMF, and DMSO and this chemistry could be a good option for preparing membranes for OSN application.

3.2. Formation, characterization and NF performance of alumina-supported polyphosphazene membrane

Fig. 3A and B show the surface and cross-sectional FE-SEM pictures

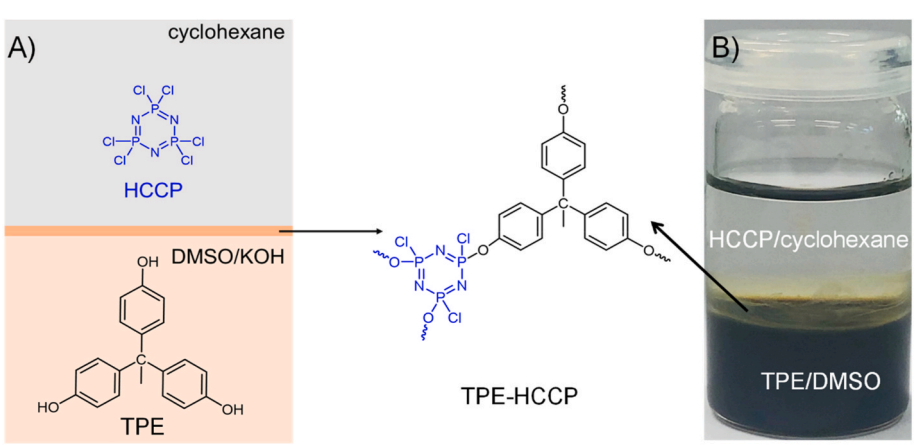

Fig. 1. A) Schematic representation of TPE-HCCP free-standing layer's formation. B) Photograph of glass vial confirming the TPE-HCCP free-standing layer's formation after 10 min.

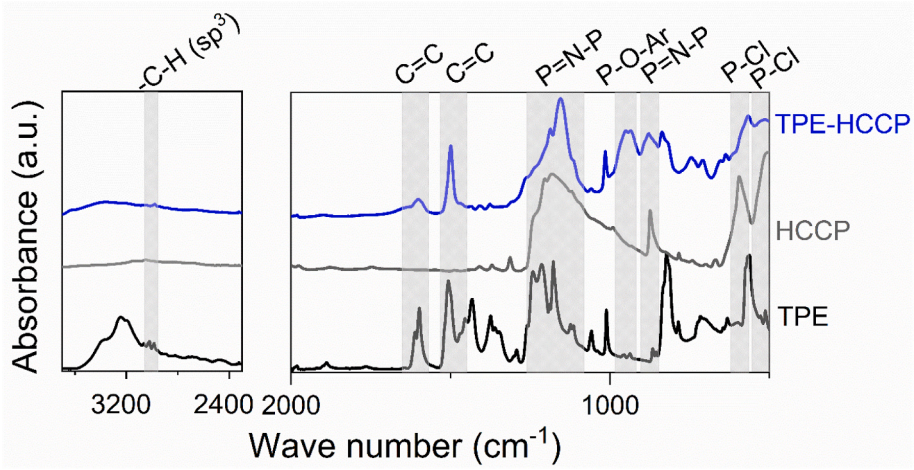

Fig. 2. FTIR spectra of monomers TPE and HCCP and the formed polyphosphazene network.

Table 1
An overview of the outcomes of several methods used for characterization of TPE-HCCP free-standing layer.

Technique	Atomic composition (%)							Number of reacted Cl		
	C	N	O	P	S	Cl	K	Based on C/N	Based on P/Cl	Based on P/C
XRF	–	–	–	34.6	5.14	39.9	20.3	–	2–3	–
CN	44.3 ± 0.2	5.6 ± 0.1	–					2–3	–	–
EDX	63.6 ± 2.2	10.2 ± 0.6	10.1 ± 0.5	7.3 ± 0.6	1 ± 0.1	5.6 ± 1.4	2.4 ± 2.1	2	3	2–3

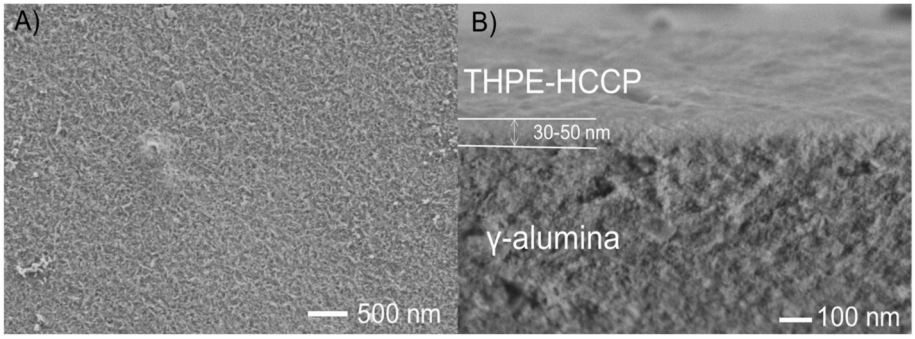

Fig. 3. A) FE-SEM picture of the TPE-HCCP membrane surface and B) Cross-section FE-SEM image.

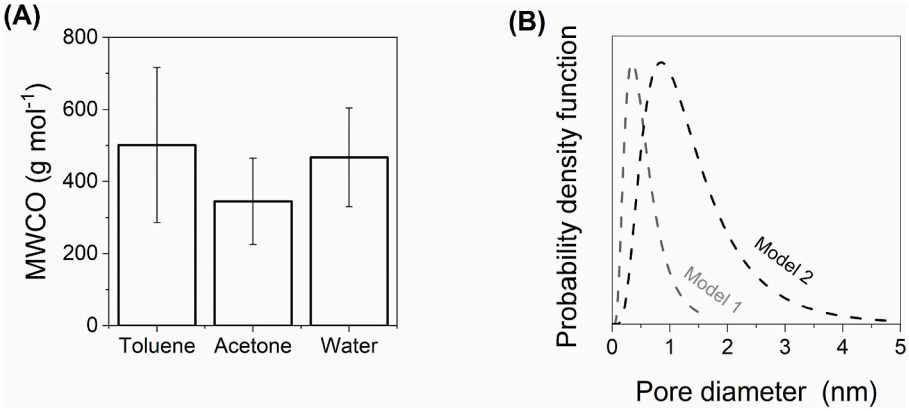

Fig. 4. (A) MWCO of alumina-supported TPE-HCCP membranes in different solvents. (B) Pore size distribution of the alumina-supported TPE-HCCP membranes calculated based on the PEG rejection in water.

of the TPE-HCCP alumina-supported membrane, respectively. Fig. 3A reveals that the surface morphology of the membrane is relatively rough and homogeneous. The cross-sectional image, Fig. 3B, shows that the thickness of the TPE-HCCP layer on top of the alumina support is between 30 and 50 nm. In contrast, cyclomatrix polyphosphazene membranes containing polyhedral oligomeric silsesquioxane (POSS-HCCP) on top of the ceramic support showed a smooth surface and a thickness of about 80 nm [45]. This difference in surface morphology between these membranes could be due to the relatively thin TPE-HCCP layer, reflecting the roughness of γ-alumina morphology rather than that of the TPE-HCCP layer itself [45]. In addition, POSS-HCCP membranes were fabricated by IP between POSS in DMSO/water and HCCP in cyclohexane, whereas TPE-HCCP networks were prepared via IP in DMSO and cyclohexane. Incorporation of water in the fabrication of the POSS-HCCP layer results in growing the layer mostly on top of the ceramic support [62]. For TPE-HCCP, the layer probably behaves differently, and the layer grows inside the pores due to the high solubility of HCCP in DMSO, explaining the differences in thickness.

Fig. 4A and Fig. S2 show the MWCO of the prepared alumina-supported TPE-HCCP membranes in different solvents. The polystyrene-based MWCO in toluene and acetone is 503 ± 215 Da and 347 ± 120 Da, respectively. Also, the PEG-based MWCO of the TPE-HCCP membrane in water was found to be 467 ± 137 Da, fitting well within the typical range of NF membranes [63]. The obtained MWCO is in the range of earlier reported IP TPE-based poly(aryl cyanurate) NF membranes (TPE-cyanuric chloride) which showed a MWCO of 400 ± 83 Da [46]. However, those TPE-cyanuric chloride based NF membranes were not developed for OSN, but for dealing with aqueous solutions at extreme pH conditions instead. Finally, the MWCO in different solvents is comparable (within the accuracy range obtained) and therefore seems to be independent of the type of solvent. It suggests that the alumina-supported TPE-HCCP membranes are suitable for solute separation in solvents, provided that the membrane shows sufficient chemical stability for the applied solvent. Furthermore, the obtained MWCO is smaller than most pharmaceutical and catalyst sizes and comparable to low MWCO OSN membranes [33,64,65].

The pore diameter of the membrane directly affects the performance of NF membranes. Cyclohexane permporometry is a technique to characterize the active pores of a membrane responsible for the actual membrane performance [48]. Fig. S3 compares the oxygen permeance of the support and TPE-HCCP membrane as a function of the relative cyclohexane pressure during the desorption step of the permporometry analysis. The data suggest a pore diameter of ~5.9 nm for the support (featuring the 3 μm γ-alumina layer on top of the 2 mm thick α-alumina disc). The pore size of the alumina-supported TPE-HCCP membranes cannot be revealed by this method since the detection limit of the set-up is 2 nm [66]. Fig. 4B shows an estimation for the pore size distribution of the alumina-supported TPE-HCCP membrane based on the two different models, the first obtained based on equations (4) and (5) giving $\mu_p = 0.5$ nm and $\sigma_p = 1.8$, and the second after correcting this mean pore diameter value for steric hindrance effects as described by equation (6), leading to $\mu_p = 1.12$ nm. Both models illustrate that pores smaller than 1 nm own the highest probability density function. As expected, the pore diameter distribution based on model 2, ranging from 0 to 5 nm, is wider than that obtained from model 1 (0–2 nm). In addition, the obtained pore size distribution based on model 1 is in line with the reported value for the other types of NF/OSN membranes, where model 1 was used to calculate pore size distribution as well [51,67].

The organic solvent nanofiltration performance of the alumina-supported TPE-HCCP membranes was evaluated by measuring the permeance of different solvents, ethanol, toluene, water, and acetone (see Fig. S4), followed by determining the rejection of salts and various dyes with different molecular weights in an aqueous solution. Fig. 5A shows the pure solvent permeance as a function of the solvent's physiochemical properties ($\delta_p\ \eta^{-1}\ V^{-1}$), where δ_p represents the Hansen solubility parameter for polarity, V is the molar volume, and η is the dynamic viscosity. A good correlation between the solvent's properties and their permeance can be observed, in line with reported results for other nanofiltration membranes [20]. As a general trend, a decrease in $\delta_p\ \eta^{-1}\ V^{-1}$ (toluene < ethanol < water < acetone) results in an increase in permeance (ethanol < toluene < acetone < water).

The average pure water permeance is 1 L m^{-2} h^{-1} bar^{-1} with a 95% CI (confidence interval) of ±0.1 L m^{-2} h^{-1} bar^{-1}, whereas for the support this is 7.1 L m^{-2} h^{-1} bar^{-1} with a 95% CI of ±1.6 L m^{-2} h^{-1} bar^{-1}. The strong reduction in the water permeance of the membrane compared to that of the support confirms the formation of a dense polymeric network. The obtained water permeance is comparable to other γ–alumina-supported TFC membranes such as polyimide (~1.7 L m^{-2} h^{-1} bar^{-1}) [66], and thioether-based membranes (~0.6 L m^{-2} h^{-1} bar^{-1}) [53], as well as PAN-supported membranes such as TPE-cyanuric chloride (1.77 L m^{-2} h^{-1} bar^{-1}) [46]. Additionally, the membrane has an acetone permeance of 0.7 L m^{-2} h^{-1} bar^{-1} and an ethanol permeance of 0.4 L m^{-2} h^{-1} bar^{-1}. The achieved ethanol and acetone permeance are moderately comparable to other IP NF membranes [65–72]. The toluene permeance is 0.55 L m^{-2} h^{-1} bar^{-1} and lower compared to the permeance of IP-prepared polymeric-supported (polyester on top of

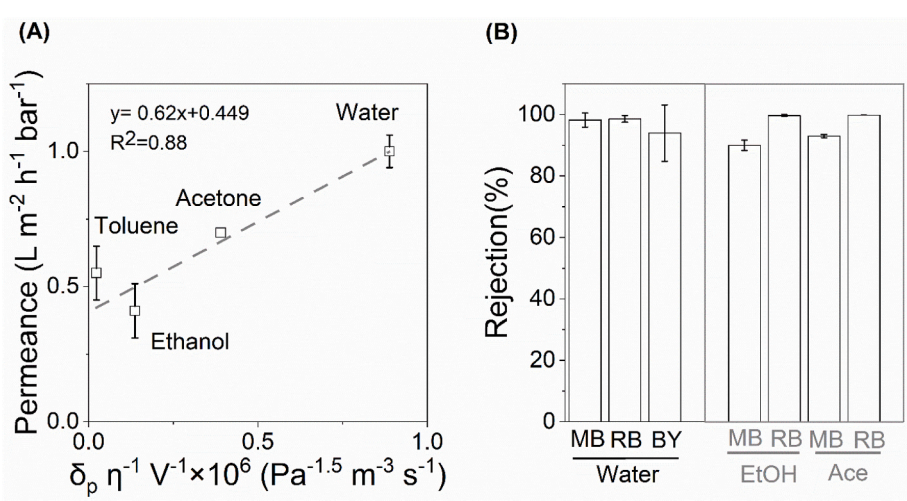

Fig. 5. *(A) Pure solvent permeance as a function of their solvent properties in terms of $\delta p\ \eta^{-1}\ V^{-1}$ for alumina-supported TPE-HCCP membranes. The gray dashed line shows the hypothetical linear relationships. (B) On the left side, the black frame: rejection of Methylene Blue (MB), Brilliant Yellow (BY), and Rhodamine B in water for TPE-HCCP membranes. On the right side, gray frame: RB and MB rejection in different solvents, ethanol(EtOH) and acetone(Ace).*

polyethylene terephthalate) membranes and similar to the permeance of other γ-alumina-supported TFC membranes prepared with grafting [33,73].

Prior to the dye rejection test, salt rejection measurements were performed for four salts to generate insights in the characteristics of the alumina supported membranes. The rejection decreases in the order Na_2SO_4 (48.6 ± 2.1%) ~ $MgCl_2$ (46.1%) > $MgSO_4$ (43.7% ± 5%) > NaCl (7.9 ± 10%), suggesting that the rejection is mainly based on dielectric exclusion, since divalent ions are retained more than monovalent ions independent of their charge [74,75]. Size exclusion may play a role as well since Na^+ has a significantly smaller size than the other ions and Cl^- is significantly smaller than Mg^{2+} [8,76] which can further explain the relatively high NaCl transport (low NaCl rejection) through the membrane. It is encouraging to compare our results with those found by You et al. [26], who prepared, to the best of our knowledge, the only other HCCP-based IP NF membranes from polyethyleneimine and HCCP. They prepared a positively charged membrane, due to the presence of remaining nitrogen groups originating from the polyethyleneimine as also found for polyethyleneimine - cyanuric chloride based NF membranes [77], with salt rejections for $MgCl_2$ (97%) > $MgSO_4$ (88%) > NaCl (87%) > Na_2SO_4 (58%) and a permeance of 3.7 L m^{-2} h^{-1} bar^{-1} when tested with a 1 g L^{-1} aqueous salt solution [26]. Although You et al. [26] did not evaluate the molecular weight cutoff or mean pore radius for their membrane, a comparison of the salt rejection measurements suggests that our selective layer on top of the alumina support is more neutral than the positively charged membrane prepared by them, as expected based on the monomers used. This lower surface charge could explain the lower salt rejections for our alumina-supported membranes [8,46]. Furthermore, our use of a solution with a higher salt concentration than You et al. [26] probably also reduced the rejection for some of the salts. Unfortunately, the surface charge for our alumina-supported TPE-HCCP membrane could not be confirmed via zeta potential measurements due to the thickness of the membrane support and equipment limitations of our zeta potential measurement equipment regarding the allowed thickness of the sample.

The performance of the alumina-supported TPE-HCCP membrane is assessed with dyes (MB, RB, and BY) rejection in water, and the result is shown in Fig. 5B. The prepared membrane has an excellent dye rejection with 98.2 ± 2.3% for MB, 98.6 ± 1.1% for RB, and 94 ± 9.2% for BY. As expected, the dye rejections of the alumina-supported TPE-HCCP membrane are enhanced substantially compared to the support with an RB rejection of 14% and BY rejection of 76% in water. It again confirms that a tight TPE-HCCP layer formed [66]. Since the difference between the MB, RB, and BY rejection is insignificant, we refrain from interpreting the rejection data in more detail. The membrane performance for RB and MB rejection in ethanol (EtOH) and acetone (Ace) is shown in Fig. 5B on the right side. The membrane has a high level of rejection for RB in ethanol and acetone, 99.7 ± 0.3% and 99.8 ± 0.0%, respectively. It is similar to the obtained RB rejection in water. However, for MB, the rejection is reduced to 92 ± 1.7% and 93 ± 0.5% in ethanol and acetone, respectively, which can be rationalized by the nature and solubility of MB in different solvents. For example, MB molecules tend to aggregate in an aqueous solution, explaining its high rejection in water compared to other solvents [78].

In summary, the rejection results show that the alumina-supported TPE-HCCP membranes can reject MB with a molecular weight of 319.8 g mol^{-1} and the smallest and longest molecular dimensions of 0.59 nm and 1.4 nm, respectively, as well as RB with a molecular weight of 479 g mol^{-1} and the smallest and longest molecular dimensions of 0.43 nm and 1.7 nm. Therefore, the swelling of the TPE-HCCP selective layer on top of alumina supports in solvents such as ethanol and acetone is restricted by the extent of cross-linking and the attachment of the layer to the support [79,80].

In Fig. 6, the performance of the alumina-supported TPE-HCCP membrane is shown in relation to the performance of other IP-based NF membranes for treating solutions containing small solutes (314 Da < M_w < 327 Da). Compared to these other IP NF membranes, alumina-supported TPE-HCCP membranes reveal acceptable permeance with good rejection (above 92%) for a small dye such as MB (with a molecular weight of 319.9 Da) in acetone and ethanol. Notably, the prepared membrane has a comparable permeance and a slightly lower rejection than polyester (4) and a polyamide (5) TFC membranes [13,31].

In summary, the new alumina supported TPE-HCCP membranes seem to be stable in solvents such as toluene, acetone, ethanol, and water with acceptable solvent permeances and good rejection for small dyes such as MB.

3.3. PAN-supported polyphosphazene

We have shown the successful formation of alumina-supported TPE-HCCP polyphosphazene membranes and their potential and performance as organic solvent nanofiltration membranes. To go one step further towards economically scaling up the membrane, we prepared TPE-HCCP membranes on a PAN support. Undoubtedly, the physical-chemical properties and structure of the support membranes significantly impact the formation and performance of composite membranes [81]. For this reason, the preparation procedure has been adapted. To evaluate the morphology, integrity, and thickness of the selective layer, FE-SEM was performed, and the results thereof are shown in Fig. 7. The FE-SEM picture confirms the formation of a layer with a few visible pinholes on top of the support, Fig. 7A. It indicates that the IP method is not sufficiently optimized, and still, some modification is needed. The PAN supports were soaked in water overnight while the ceramic supports were kept dry before IP. The observed defects could be due to the

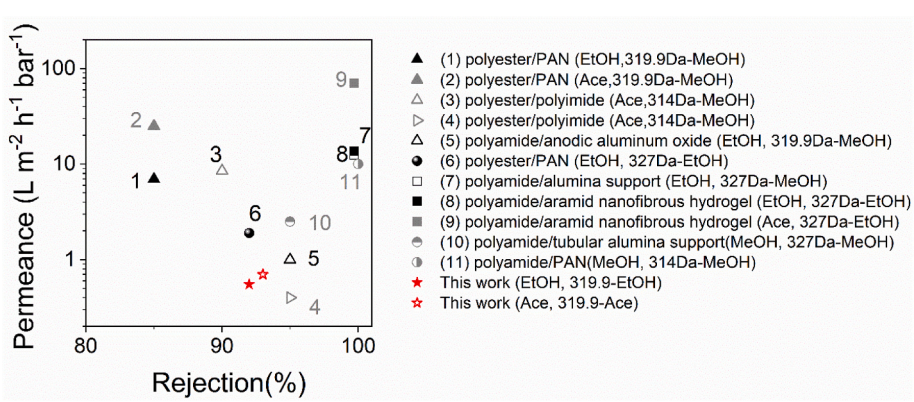

Fig. 6. *Comparison of the prepared alumina-supported TPE-HCCP membrane performance for small solutes (*314 Da < *Mw* < *327.*3 Da*) from this work with other IP NF membranes reported in open literature* [10,13,31,32,34–36,38]. *The legend for each membrane shows polymer type/support type (Solvent for permeance measurement, Mw of solute-solvent used to measure the rejection of solute).*

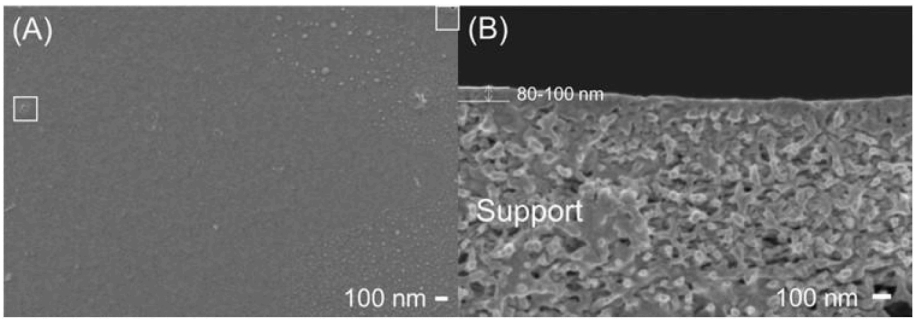

Fig. 7. FE-SEM pictures of the PAN-based TPE-HCCP membrane (A) surface and B) Cross-section. The white squares show the pinholes on the surface of PAN-supported membranes.

presence of trapped water in the pores of PAN support during IP, which hinders the formation of the CPPz layer on top of the support. Another reason could be the limited resistance of the PAN support to the DMSO solution, which could have resulted in the formation of defects upon its exposure to the phenolate/DMSO solution. Efforts to prepare PAN-supported membranes based on the procedure used for alumina-supported membranes failed (the PAN top layer was removed) due to the low thermal resistance of the PAN support, making it impossible to pour the phenolate solution on top of the support at 80 °C. Fig. 7B shows the cross-sectional image of the TFCs membranes. The formed layer on top of the PAN support is in a range of 80–100 nm (see Fig. 7B), and, therefore, thicker than the obtained TPE-HCCP layer on the alumina support (see Fig. 3).

The NF performance of the PAN-supported TPE-HCCP membrane, assessed by measuring the permeance of water, acetone, and ethanol, as well as the rejection of different salts, is shown in Fig. 8. For the PAN-supported TPE-HCCP membrane, the solvent permeance as a function of its physiochemical properties ($\delta_p\ \eta^{-1}\ V^{-1}$) follows the same order as that for the alumina-supported membranes; the permeance enhances as $\delta_p\ \eta^{-1}\ V^{-1}$ increases (Fig. 8A). This indicates comparable interaction between the polymeric network and the solvents for both membranes. Although the TPE-HCCP layer of the prepared PAN-supported membranes is thicker, these membranes show considerably higher water and acetone permeances (around 1.2 and 2.6 L m^{-2} h^{-1} bar^{-1}, respectively) than the alumina-supported TPE-HCCP membranes. However, the ethanol permeance for the PAN-supported TPE-HCCP membrane is lower, with an ethanol permeance of around 0.2 L m^{-2} h^{-1} bar^{-1}.

The results of the salt rejection measurements for three different salts in single salt aqueous solution experiments are shown in Fig. 8B. The salt rejection follows the order of Na_2SO_4 (71.1%) > $MgSO_4$ (46.2%) ~ NaCl (46%). Before heat treatment, PAN-supported membranes show a Na_2SO_4 rejection of 43%, indicating the effectiveness of heat treatment in the preparation of these membranes. The lower rejection of $MgSO_4$ compared to Na_2SO_4 indicates that the separation is based on a negative charge repulsion (Donnan-exclusion). Zeta potential results confirm the formation of a negative charge layer on top of the PAN support (Fig. S5). Also, it illustrates that over the pH range from 3.9 to 9, the zeta potential of the layer remains negative, indicating that the isoelectric point (IEP) of the membrane surface is below 3.9, and the value depends on the solution pH as normally found. It should be noted that both the absolute zeta potential value as well as the slope of the zeta potential with pH are lower than found for typical commercial polyamide membranes such as NF-270 [82]. It is good to mention that a negative charge of the membrane might be due to the presence of unreacted phenolate of TPE in the network. Although the PAN-supported membrane shows a higher salt rejection than the alumina-supported membranes, the rejection is lower than reported for other TFC membranes [46]. If Donnan-exclusion based on the negatively charged membrane surface would be the major contributor to the separation mechanism, it would be expected that $MgSO_4$ would have been rejected to a larger extent than NaCl, due to the stronger repulsion of SO_4^{2-} compared to Cl^- by the negatively charged surface of the membrane [76]. However, it should be noted that for all salts 2 g L^{-1} solutions we used, leading to a relatively high ionic strength for the $MgSO_4$ solution compared to the ionic strengths of the Na_2SO_4 solution and especially the NaCl solution. This relatively low ionic strength for the applied NaCl solution may have led to relatively low charge shielding and consequently higher rejections than obtained when applying ionic strength NaCl solutions similar to the ionic strength of the

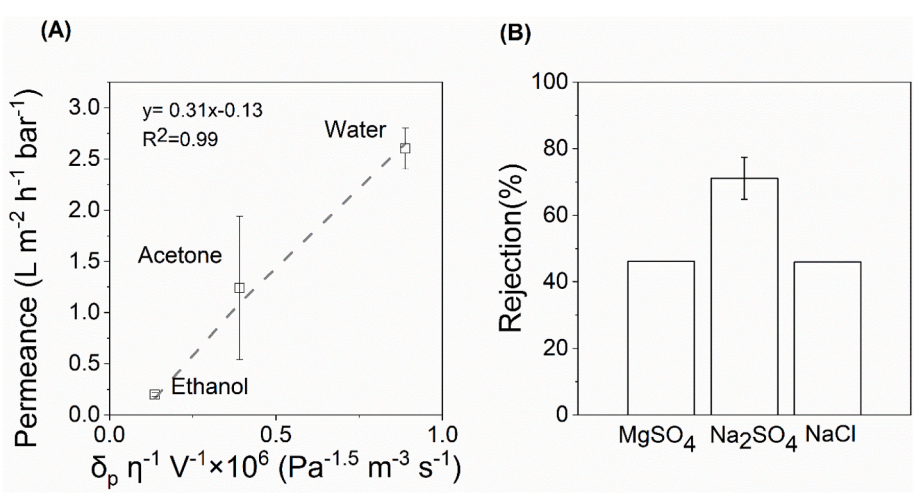

Fig. 8. *(A) Pure solvent permeance as a function of their solvent properties in terms of $\delta_p\ \eta^{-1}V^{-1}$ for* PAN-supported *TPE-HCCP membranes. The gray dashed line shows the hypothetical linear relationships (B) Salt rejection for three different salts.*

$MgSO_4$ solution used [83]. Furthermore, results from MWCO experiments show that the rejection does not reach 100% for all tested 3 membrane samples (Fig. S6), confirming the presence of the pinholes. This relatively high MWCO for the PAN supported membranes compared to the low MWCO of the alumina supported membranes may have (negatively) affected the Mg^{2+} rejection to a larger extent than the rejection of the smaller Na^+. The higher Na_2SO_4 and NaCl rejections for the more open and negatively charged PAN-supported TPE-HCCP membrane compared to the alumina-supported TPE-HCCP membrane and the similar $MgSO_4$ rejections for the PAN-supported and alumina-supported membranes supports our impression that the alumina-supported membrane has a more neutral surface than the negatively charged PAN-supported TPE-HCCP membrane. Also, the RB rejection in water for the PAN-supported TPE-HCCP membranes is only about 50%. Although the lower rejection compared to the alumina-supported TPE-HCCP membrane could partly be caused by the negative charge of the PAN-supported TPE-HCCP membrane, it is more likely that the presence of pinholes for this latter membrane negatively affected the rejection for this cation as well. These rejections can probably be improved by modifying the IP method to form an integrated defect-free selective layer.

These obtained results suggest that the properties of the formed layer depend strongly on the properties of the support. The obtained differences in layer formation and characteristics can be due to the lower hydrophilicity of the PAN support or, more importantly, the significant difference in the pore size of the supports. The ceramic support has a γ-alumina layer with a pore diameter of 5.9 nm on top, while the mean pore size of the PAN support is 54.3 nm [43]. The small pores of supports favor forming a high cross-linking degree. When the support is soaked in the first IP monomer solution, a substantial amount of monomers is trapped in the bigger pores of supports. After exposing the surface to the second solution, the polymer grows in the inner pores more, which hinders the diffusion of monomers to the reaction zone and makes a defective low cross-linked layer [81]. This result is in line with the finding of Sharabati et al. [84]. They found that increasing the pore size of the support decreases salt rejection, reduces cross-linking extent, and increases water permeation. Finally, each support provides a different interface for IP that influences the attachment of the IP-formed selective layer to the support and dictates the performance and stability of the membrane in each solvent. Our future research will focus on adapting techniques for preparing TPE-HCCP networks on polymeric supports to enhance membrane integration and rejection.

In summary, although the new TPE-HCCP polyphosphazene membrane is successfully formed on top of alumina supports, for PAN-supported TFC membranes the IP method and/or the chemical stability of the PAN support needs to be updated and improved to prepare a better performing membrane, and additional efforts are required to develop a proper CPPz layer on top of polymeric supports. A solution for potential insufficient chemical stability of the PAN support in DMSO has recently been proposed by Yushkin et al. [85], who showed that the use of infrared heating at 170 °C strongly increases the stability of porous PAN in aprotic solvents such as DMSO.

4. Conclusions

In this work, we show for the first time the preparation of polyphosphazene TFC membranes via IP of TPE and HCCP on top of a ceramic support for OSN application. FE-SEM has confirmed the formation of a defect-free network atop the ceramic support with a film thickness of 30–50 nm. The resulting TPE-HCCP network is highly cross-linked and shows performance in the NF range, making the membrane suitable for OSN application. Alumina supported TPE-HCCP membranes exhibit a high MB (Mw of 319.8 g mol^{-1}) rejection of 98.2 ± 2.3% in water, 92 ± 1.7% in ethanol, and 93 ± 0.5% in acetone while maintaining acceptable permeance. Also, the obtained PEG-based MWCO in water and polystyrene-based MWCO in acetone and toluene are comparable and between 300 and 500 Da. Furthermore, aiming for more cost-effective production of TPE-HCCP NF membranes, the TPE-HCCP layer was formed with IP on top of a PAN support. FE-SEM has revealed the formation of a 80–100 nm layer with a few pinholes on top of the PAN support. The water and acetone permeance of TPE-HCCP PAN-supported membranes is higher compared to alumina-supported membranes. However, these higher permeances can (partly) be due to the presence of the pinholes. The resulting TPE-HCCP PAN-supported membrane is negatively charged, resulting in a higher rejection of salts. However, a proper MWCO could not be determined, most likely due to the pinholes present in the TFC layer. Finally, additional attempts are needed to prepare defect-free cyclomatrix polyphophazene TFCs on top of the PAN supports. One of the possibilities to improve these PAN-supported membranes is the use of recently reported infrared heat-treated PAN supports with improved chemical stability for DMSO. Our work is among the first attempts to design and evaluate the potential of cyclomatric polyphosphazene networks as a membrane for OSN. It clearly shows that this network has the potential to be used as an alternative to conventional TFC OSN membranes.

Author statement

Farzaneh Radmanesh: Conceptualization, Investigation, Data curation, Validation, Methodology, Writing - original draft. **Gerrald Bargeman**: Conceptualization, Data curation, Supervision, Writing - Review & Editing. **Nieck E. Benes:** Conceptualization, Project administration, Funding acquisition, Supervision, Writing - Review & Editing.

Declaration of competing interest

The authors declare that they have no known competing financial interests or personal relationships that could have appeared to influence the work reported in this paper.

Data availability

Data will be made available on request.

Acknowledgements

This work is part of the GENESIS project and the authors acknowledge the financial support from the European Union's Horizon 2020 Research and Innovation Program under the Grant Agreement No. 760899. The authors would like to thank Moritz Junker from Membrane Science and Technology group at the University of Twente, Wouter Nielen from The European Membrane Institute Twente, and Tao Wang from the Membrane Science and Technology group at the University of Twente for their contribution to partly performing and analyzing MWCO and zeta potential measurements. The authors thank Circa Group for kindly providing the Cyrene.

Appendix A. Supplementary data

Supplementary data to this article can be found online at https://doi.org/10.1016/j.memsci.2022.121215.

References

[1] Y. Li, Z. Guo, S. Li, B. Van der Bruggen, Interfacially polymerized thin-film composite membranes for organic solvent nanofiltration, Adv. Mater. Interfac. 8 (2021), 2001671, https://doi.org/10.1002/admi.202001671.

[2] P. Li, H. Lan, K. Chen, X. Ma, B. Wei, M. Wang, P. Li, Y. Hou, Q. Jason Niu, Novel high-flux positively charged aliphatic polyamide nanofiltration membrane for selective removal of heavy metals, Separ. Purif. Technol. 280 (2022), 119949, https://doi.org/10.1016/j.seppur.2021.119949.

[3] K. Nath, H.K. Dave, T.M. Patel, Revisiting the recent applications of nanofiltration in food processing industries: progress and prognosis, Trends Food Sci. Technol. 73 (2018) 12–24, https://doi.org/10.1016/j.tifs.2018.01.001.

[4] E. Schäfer, Andrea Iris, Anthony G. Fane, Nanofiltration: Principles, Applications, and New Materials, John Wiley & Sons, Inc., 2021.
[5] S. Chisca, V.-E. Musteata, W. Zhang, S. Vasylevskyi, G. Falca, E. Abou-Hamad, A.-H. Emwas, M. Altunkaya, S.P. Nunes, Polytriazole membranes with ultrathin tunable selective layer for crude oil fractionation, Science 376 (2022) 1105–1110, https://doi.org/10.1126/science.abm7686, 80-.
[6] Y. Zhao, T. Tong, X. Wang, S. Lin, E.M. Reid, Y. Chen, Differentiating solutes with precise nanofiltration for next generation environmental separations: a review, Environ. Sci. Technol. 55 (2021) 1359–1376, https://doi.org/10.1021/acs.est.0c04593.
[7] G. Bargeman, J.B. Westerink, O. Guerra Miguez, M. Wessling, The effect of NaCl and glucose concentration on retentions for nanofiltration membranes processing concentrated solutions, Separ. Purif. Technol. 134 (2014) 46–57, https://doi.org/10.1016/j.seppur.2014.07.025.
[8] G. Bargeman, J.B. Westerink, C.F.H. Manuhutu, A. ten Kate, The effect of membrane characteristics on nanofiltration membrane performance during processing of practically saturated salt solutions, J. Membr. Sci. 485 (2015) 112–122, https://doi.org/10.1016/j.memsci.2015.03.039.
[9] M.F. Jimenez Solomon, Y. Bhole, A.G. Livingston, High flux membranes for organic solvent nanofiltration (OSN)—interfacial polymerization with solvent activation, J. Membr. Sci. (2012) 371–382, https://doi.org/10.1016/j.memsci.2012.08.030, 423–424.
[10] S. Karan, Z. Jiang, A.G. Livingston, Sub–10 nm polyamide nanofilms with ultrafast solvent transport for molecular separation, Science 348 (2015) 1347–1351, https://doi.org/10.1126/science.aaa5058, 80-.
[11] K.S. Goh, J.Y. Chong, Y. Chen, W. Fang, T.-H. Bae, R. Wang, Thin-film composite hollow fibre membrane for low pressure organic solvent nanofiltration, J. Membr. Sci. 597 (2020), 117760, https://doi.org/10.1016/j.memsci.2019.117760.
[12] J. Liu, S. Wang, T. Huang, P. Manchanda, E. Abou-Hamad, S.P. Nunes, Smart covalent organic networks (CONs) with "on-off-on" light-switchable pores for molecular separation, Sci. Adv. 6 (2020), https://doi.org/10.1126/sciadv.abb3188.
[13] M.F. Jimenez-Solomon, Q. Song, K.E. Jelfs, M. Munoz-Ibanez, A.G. Livingston, Polymer nanofilms with enhanced microporosity by interfacial polymerization, Nat. Mater. 15 (2016) 760–767, https://doi.org/10.1038/nmat4638.
[14] J. Li, J.-L. Gong, G.-M. Zeng, B. Song, W.-C. Cao, S.-Y. Fang, S.-Q. Tang, Y. Guan, Z.-K. Tan, Z.-P. Chen, X.-Q. Mao, R.-L. Zhu, Thin-film composite polyester nanofiltration membrane with high flux and efficient dye/salts separation fabricated from precise molecular sieving structure of β-cyclodextrin, Separ. Purif. Technol. 276 (2021), 119352, https://doi.org/10.1016/j.seppur.2021.119352.
[15] N.A. Khan, R. Zhang, H. Wu, J. Shen, J. Yuan, C. Fan, L. Cao, M.A. Olson, Z. Jiang, Solid–vapor interface engineered covalent organic framework membranes for molecular separation, J. Am. Chem. Soc. 142 (2020) 13450–13458, https://doi.org/10.1021/jacs.0c04589.
[16] M.H. Abdellah, L. Pérez-Manríquez, T. Puspasari, C.A. Scholes, S.E. Kentish, K.-V. Peinemann, A catechin/cellulose composite membrane for organic solvent nanofiltration, J. Membr. Sci. 567 (2018) 139–145, https://doi.org/10.1016/j.memsci.2018.09.042.
[17] M.F. Jimenez-Solomon, P. Gorgojo, M. Munoz-Ibanez, A.G. Livingston, Beneath the surface: influence of supports on thin film composite membranes by interfacial polymerization for organic solvent nanofiltration, J. Membr. Sci. 448 (2013) 102–113, https://doi.org/10.1016/j.memsci.2013.06.030.
[18] G.M. Shi, Y. Feng, B. Li, H.M. Tham, J.-Y. Lai, T.-S. Chung, Recent progress of organic solvent nanofiltration membranes, Prog. Polym. Sci. 123 (2021), 101470, https://doi.org/10.1016/j.progpolymsci.2021.101470.
[19] M. Amirilargani, G.N. Yokota, G.H. Vermeij, R.B. Merlet, G. Delen, L.D. B. Mandemaker, B.M. Weckhuysen, L. Winnubst, A. Nijmeijer, L.C.P.M. Smet, E.J. R. Sudhölter, Melamine-based microporous organic framework thin films on an alumina membrane for high-flux organic solvent nanofiltration, ChemSusChem 13 (2020) 136–140, https://doi.org/10.1002/cssc.201902341.
[20] A. Asadi Tashvigh, N.E. Benes, Covalent organic polymers for aqueous and organic solvent nanofiltration, Separ. Purif. Technol. 298 (2022), 121589, https://doi.org/10.1016/j.seppur.2022.121589.
[21] R.S. Ullah, L. Wang, H. Yu, N.M. Abbasi, M. Akram, Z. ul-Abdin, M. Saleem, M. Haroon, R.U. Khan, Synthesis of polyphosphazenes with different side groups and various tactics for drug delivery, RSC Adv. 7 (2017) 23363–23391, https://doi.org/10.1039/C6RA27103K.
[22] H.R. Allcock, Recent developments in polyphosphazene materials science, Curr. Opin. Solid State Mater. Sci. 10 (2006) 231–240, https://doi.org/10.1016/j.cossms.2007.06.001.
[23] K.S. Ogueri, H.R. Allcock, C.T. Laurencin, Generational biodegradable and regenerative polyphosphazene polymers and their blends with poly (lactic-co-glycolic acid), Prog. Polym. Sci. 98 (2019), 101146, https://doi.org/10.1016/j.progpolymsci.2019.101146.
[24] H.R. Allcock, N.J. Sunderland, R. Ravikiran, J.M. Nelson, Polyphosphazenes with novel architectures: influence on physical properties and behavior as solid polymer electrolytes, Macromolecules 31 (1998) 8026–8035, https://doi.org/10.1021/ma9804491.
[25] W. Wei, X. Huang, K. Chen, Y. Tao, X. Tang, Fluorescent organic–inorganic hybrid polyphosphazene microspheres for the trace detection of nitroaromatic explosives, RSC Adv. 2 (2012) 3765, https://doi.org/10.1039/c2ra20263h.
[26] M. You, W. Li, Y. Pan, P. Fei, H. Wang, W. Zhang, L. Zhi, J. Meng, Preparation and characterization of antibacterial polyamine-based cyclophosphazene nanofiltration membranes, J. Membr. Sci. 592 (2019), 117371, https://doi.org/10.1016/j.memsci.2019.117371.
[27] C.A. Allen, D.G. Cummings, A.E. Grey, R.E. McAtee, R.R. McCaffrey, Separation of Cr ions from Co and mn ions by poly (bis(phenoxy) phosphazene) membranes, J. Membr. Sci. 33 (1987) 181–189, https://doi.org/10.1016/S0376-7388(00)80376-2.
[28] M.M.A. Almijbilee, X. Wu, A. Zhou, X. Zheng, X. Cao, W. Li, Polyetheramide organic solvent nanofiltration membrane prepared via an interfacial assembly and polymerization procedure, Separ. Purif. Technol. 234 (2020), 116033, https://doi.org/10.1016/j.seppur.2019.116033.
[29] Q. Liu, X. Wu, K. Zhang, Polysulfone/Polyamide-SiO2 composite membrane with high permeance for organic solvent nanofiltration, Membranes 8 (2018) 89, https://doi.org/10.3390/membranes8040089.
[30] M.H. Abdellah, L. Pérez-Manríquez, T. Puspasari, C.A. Scholes, S.E. Kentish, K.-V. Peinemann, Effective interfacially polymerized polyester solvent resistant nanofiltration membrane from bioderived materials, Adv. Sustain. Syst. 2 (2018), 1800043, https://doi.org/10.1002/adsu.201800043.
[31] C. Liu, J. Yang, B. Guo, S. Agarwal, A. Greiner, Z. Xu, Interfacial polymerization at the alkane/ionic liquid interface, Angew. Chem. 133 (2021) 14757–14764, https://doi.org/10.1002/ange.202103555.
[32] L.F. Villalobos, T. Huang, K.-V. Peinemann, Cyclodextrin films with fast solvent transport and shape-selective permeability, Adv. Mater. 29 (2017), 1606641, https://doi.org/10.1002/adma.201606641.
[33] S.H. Park, A. Alammar, Z. Fulop, B.A. Pulido, S.P. Nunes, G. Szekely, Hydrophobic thin film composite nanofiltration membranes derived solely from sustainable sources, Green Chem. 23 (2021) 1175–1184, https://doi.org/10.1039/d0gc03226c.
[34] T. Huang, T. Puspasari, S.P. Nunes, K. Peinemann, Ultrathin 2D-layered cyclodextrin membranes for high- performance organic solvent nanofiltration, Adv. Funct. Mater. 30 (2020), 1906797, https://doi.org/10.1002/adfm.201906797.
[35] Y. Li, E. Wong, A. Volodine, C. Van Haesendonck, K. Zhang, B. Van der Bruggen, Nanofibrous hydrogel composite membranes with ultrafast transport performance for molecular separation in organic solvents, J. Mater. Chem. A. 7 (2019) 19269–19279, https://doi.org/10.1039/C9TA06169J.
[36] L. Xia, J. Ren, M. Weyd, J.R. McCutcheon, Ceramic-supported thin film composite membrane for organic solvent nanofiltration, J. Membr. Sci. 563 (2018) 857–863, https://doi.org/10.1016/j.memsci.2018.05.069.
[37] S. Sorribas, P. Gorgojo, C. Téllez, J. Coronas, A.G. Livingston, High flux thin film nanocomposite membranes based on metal–organic frameworks for organic solvent nanofiltration, J. Am. Chem. Soc. 135 (2013) 15201–15208, https://doi.org/10.1021/ja407665w.
[38] Z. Ali, B.S. Ghanem, Y. Wang, F. Pacheco, W. Ogieglo, H. Vovusha, G. Genduso, U. Schwingenschlögl, Y. Han, I. Pinnau, Finely tuned submicroporous thin-film molecular sieve membranes for highly efficient fluid separations, Adv. Mater. 32 (2020), 2001132, https://doi.org/10.1002/adma.202001132.
[39] F. Radmanesh, E.J.R. Sudhölter, A. Tena, M.G. Elshof, N.E. Benes, Thin film composite cyclomatrix poly(phenoxy)phosphazenes membranes for hot hydrogen separation, Adv. Mater. Interfac.. ((n.d.)). in press.
[40] F. Radmanesh, A. Tena, E.J.R. Sudhölter, M.A. Hempenius, N.E. Benes, Non-aqueous Interfacial Polymerization Derived Polyphosphazene Films for Sieving or Blocking Hydrogen Gas, Submitted. (n.d.).
[41] M. ten Hove, M.W.J. Luiten-Olieman, C. Huiskes, A. Nijmeijer, L. Winnubst, Hydrothermal stability of silica, hybrid silica and Zr-doped hybrid silica membranes, Separ. Purif. Technol. 189 (2017) 48–53, https://doi.org/10.1016/j.seppur.2017.07.045.
[42] S. Roy Chowdhury, K. Keizer, J.E. ten Elshof, D.H.A. Blank, Effect of trace amounts of water on organic solvent transport through γ-alumina membranes with varying pore sizes, Langmuir 20 (2004) 4548–4552, https://doi.org/10.1021/la0364237.
[43] Y. Ma, S. Velioğlu, Z. Yin, R. Wang, J.W. Chew, Molecular dynamics investigation of membrane fouling in organic solvents, J. Membr. Sci. 632 (2021), 119329, https://doi.org/10.1016/j.memsci.2021.119329.
[44] T.H. Lee, M.G. Shin, J.G. Jung, E.H. Suh, J.G. Oh, J.H. Kang, B.S. Ghanem, J. Jang, J.-H. Lee, I. Pinnau, H.B. Park, Facile suppression of intensified plasticization in glassy polymer thin films towards scalable composite membranes for propylene/propane separation, J. Membr. Sci. 645 (2022), 120215, https://doi.org/10.1016/j.memsci.2021.120215.
[45] F. Radmanesh, M.G. Elshof, N.E. Benes, Polyoctahedral silsesquioxane hexachlorocyclotriphosphazene membranes for hot gas separation, ACS Appl. Mater. Interfaces 13 (2021) 8960–8966, https://doi.org/10.1021/acsami.0c21968.
[46] M.G. Elshof, E. Maaskant, M.A. Hempenius, N.E. Benes, Poly(aryl cyanurate)-based thin-film composite nanofiltration membranes, ACS Appl. Polym. Mater. 3 (2021) 2385–2392, https://doi.org/10.1021/acsapm.0c01366.
[47] F. Radmanesh, M. Pilz, L. Ansaloni, T.A. Peters, E. Louradour, H. van Veen, D. Høvik, M.A. Hempenius, N.E. Benes, Comparing amine- and ammonium functionalized silsesquioxanes for large scale synthesis of hybrid polyimide high-temperature gas separation membranes, J. Membr. Sci. 637 (2021), 119524, https://doi.org/10.1016/j.memsci.2021.119524.
[48] F.P. Cuperus, D. Bargeman, C.A. Smolders, Permporometry: the determination of the size distribution of active pores in UF membranes, J. Membr. Sci. 71 (1992) 57–67, https://doi.org/10.1016/0376-7388(92)85006-5.
[49] D.M. Reurink, J.P. Haven, I. Achterhuis, S. Lindhoud, E.H.D.W. Roesink, W.M. de Vos, Annealing of polyelectrolyte multilayers for control over ion permeation, Adv. Mater. Interfac. 5 (2018), 1800651, https://doi.org/10.1002/admi.201800651.
[50] M.G. Elshof, W.M. de Vos, J. de Grooth, N.E. Benes, On the long-term pH stability of polyelectrolyte multilayer nanofiltration membranes, J. Membr. Sci. 615 (2020), 118532, https://doi.org/10.1016/j.memsci.2020.118532.

[51] A. Asadi Tashvigh, M.G. Elshof, N.E. Benes, Development of thin-film composite membranes for nanofiltration at extreme pH, ACS Appl. Polym. Mater. 3 (2021) 5912–5919, https://doi.org/10.1021/acsapm.1c01172.
[52] P. Puhlfürß, A. Voigt, R. Weber, M. Morbé, Microporous TiO2 membranes with a cut off <500 Da, J. Membr. Sci. 174 (2000) 123–133, https://doi.org/10.1016/S0376-7388(00)00380-X.
[53] N. Kyriakou, R.B. Merlet, J.D. Willott, A. Nijmeijer, L. Winnubst, M.-A. Pizzoccaro-Zilamy, New method toward a robust covalently attached cross-linked nanofiltration membrane, ACS Appl. Mater. Interfaces 12 (2020) 47948–47956, https://doi.org/10.1021/acsami.0c13339.
[54] B. Sutariya, S. Karan, A realistic approach for determining the pore size distribution of nanofiltration membranes, Separ. Purif. Technol. 293 (2022), 121096, https://doi.org/10.1016/j.seppur.2022.121096.
[55] K.H. Youm, W.S. Kim, Prediction of intrinsic pore properties of ultrafiltration membrane by solute rejection curves: effects of operating conditions on pore properties, J. Chem. Eng. Jpn. 24 (1991) 1–7, https://doi.org/10.1252/jcej.24.1.
[56] J.A.V. Donald, L. Pavia, Gary M. Lampman, George S. Kriz, Introduction to Spectroscopy, Cengage learning, 2014.
[57] F. Alregeb, F. Khalili, B. Sweileh, D.K. Ali, Synthesis and characterization of chelating hyperbranched polyester nanoparticles for Cd(II) ion removal from water, Molecules 27 (2022) 3656, https://doi.org/10.3390/molecules27123656.
[58] A. Deniz, N. Zaytoun, L. Hetjens, A. Pich, Polyphosphazene–tannic acid colloids as building blocks for bio-based flame-retardant coatings, ACS Appl. Polym. Mater. 2 (2020) 5345–5351, https://doi.org/10.1021/acsapm.0c00574.
[59] E. Maaskant, H. Gojzewski, M.A. Hempenius, G.J. Vancso, N.E. Benes, Thin cyclomatrix polyphosphazene films: interfacial polymerization of hexachlorocyclotriphosphazene with aromatic biphenols, Polym. Chem. 9 (2018) 3169–3180, https://doi.org/10.1039/C8PY00444G.
[60] Luo Jiang Wang, Qiao Qi, Wang Zou, Design and application of highly efficient flame retardants for polycarbonate combining the advantages of cyclotriphosphazene and silicone oil, Polymers 11 (2019) 1155, https://doi.org/10.3390/polym11071155.
[61] Y. Zhang, X. Chen, J. Xu, Q. Zhang, L. Gao, Z. Wang, L. Qu, K. Wang, Y. Li, Z. Cai, Y. Zhao, C. Yang, Cross-linked polyphosphazene nanospheres boosting long-lived organic room-temperature phosphorescence, J. Am. Chem. Soc. 144 (2022) 6107–6117, https://doi.org/10.1021/jacs.2c02076.
[62] Y. Zhang, N.E. Benes, R.G.H. Lammertink, Visualization and characterization of interfacial polymerization layer formation, Lab Chip 15 (2015) 575–580, https://doi.org/10.1039/C4LC01046A.
[63] P. Marchetti, M.F. Jimenez Solomon, G. Szekely, A.G. Livingston, Molecular separation with organic solvent nanofiltration: a critical review, Chem. Rev. 114 (2014) 10735–10806, https://doi.org/10.1021/cr500006j.
[64] J. Geens, B. De Witte, B. Van der Bruggen, Removal of API's (active pharmaceutical ingredients) from organic solvents by nanofiltration, Separ. Sci. Technol. 42 (2007) 2435–2449, https://doi.org/10.1080/01496390701477063.
[65] A. Asadi Tashvigh, T.-S. Chung, Robust polybenzimidazole (PBI) hollow fiber membranes for organic solvent nanofiltration, J. Membr. Sci. 572 (2019) 580–587, https://doi.org/10.1016/j.memsci.2018.11.048.
[66] N. Kyriakou, L. Winnubst, M. Drobek, S. de Beer, A. Nijmeijer, M.-A. Pizzoccaro-Zilamy, Controlled nanoconfinement of polyimide networks in mesoporous γ-alumina membranes for the molecular separation of organic dyes, ACS Appl. Nano Mater. 4 (2021) 14035–14046, https://doi.org/10.1021/acsanm.1c03322.
[67] S. Yang, H. Li, X. Zhang, S. Du, J. Zhang, B. Su, X. Gao, B. Mandal, Amine-functionalized ZIF-8 nanoparticles as interlayer for the improvement of the separation performance of organic solvent nanofiltration (OSN) membrane, J. Membr. Sci. 614 (2020), 118433, https://doi.org/10.1016/j.memsci.2020.118433.
[68] Z. Zhou, D. Lu, X. Li, L.M. Rehman, A. Roy, Z. Lai, Fabrication of highly permeable polyamide membranes with large "leaf-like" surface nanostructures on inorganic supports for organic solvent nanofiltration, J. Membr. Sci. 601 (2020), 117932, https://doi.org/10.1016/j.memsci.2020.117932.
[69] Y. Chen, M. Toth, C. He, Facile and fast fabrication of high structure-stable thin film nanocomposite membrane for potential application in solvent resistance nanofiltration, Appl. Surf. Sci. 496 (2019), 143483, https://doi.org/10.1016/j.apsusc.2019.07.225.
[70] X. Cheng, X. Jiang, Y. Zhang, C.H. Lau, Z. Xie, D. Ng, S.J.D. Smith, M.R. Hill, L. Shao, Building additional passageways in polyamide membranes with hydrostable metal organic frameworks to recycle and remove organic solutes from various solvents, ACS Appl. Mater. Interfaces 9 (2017) 38877–38886, https://doi.org/10.1021/acsami.7b07373.
[71] Y. Zhang, X. Cheng, X. Jiang, J.J. Urban, C.H. Lau, S. Liu, L. Shao, Robust natural nanocomposites realizing unprecedented ultrafast precise molecular separations, Mater. Today 36 (2020) 40–47, https://doi.org/10.1016/j.mattod.2020.02.002.
[72] Z. Yuan, X. Wu, Y. Jiang, Y. Li, J. Huang, L. Hao, J. Zhang, J. Wang, Carbon dots-incorporated composite membrane towards enhanced organic solvent nanofiltration performance, J. Membr. Sci. 549 (2018) 1–11, https://doi.org/10.1016/j.memsci.2017.11.051.
[73] M. Amirilargani, R.B. Merlet, A. Nijmeijer, L. Winnubst, L.C.P.M. de Smet, E.J. R. Sudhölter, Poly (maleic anhydride-alt-1-alkenes) directly grafted to γ-alumina for high-performance organic solvent nanofiltration membranes, J. Membr. Sci. 564 (2018) 259–266, https://doi.org/10.1016/j.memsci.2018.07.042.
[74] J. de Grooth, R. Oborný, J. Potreck, K. Nijmeijer, W.M. de Vos, The role of ionic strength and odd–even effects on the properties of polyelectrolyte multilayer nanofiltration membranes, J. Membr. Sci. 475 (2015) 311–319, https://doi.org/10.1016/j.memsci.2014.10.044.
[75] D.L. Oatley, L. Llenas, R. Pérez, P.M. Williams, X. Martínez-Lladó, M. Rovira, Review of the dielectric properties of nanofiltration membranes and verification of the single oriented layer approximation, Adv. Colloid Interface Sci. 173 (2012) 1–11, https://doi.org/10.1016/j.cis.2012.02.001.
[76] J. Luo, Y. Wan, Effects of pH and salt on nanofiltration—a critical review, J. Membr. Sci. 438 (2013) 18–28, https://doi.org/10.1016/j.memsci.2013.03.029.
[77] K.P. Lee, J. Zheng, G. Bargeman, A.J.B. Kemperman, N.E. Benes, pH stable thin film composite polyamine nanofiltration membranes by interfacial polymerisation, J. Membr. Sci. 478 (2015) 75–84, https://doi.org/10.1016/j.memsci.2014.12.045.
[78] J.A. Caram, J.F.M. Suárez, A.M. Gennaro, M.V. Mirífico, Electrochemical behaviour of methylene blue IN NON-aqueous solvents, Electrochim. Acta 164 (2015) 353–363, https://doi.org/10.1016/j.electacta.2015.01.196.
[79] J. Canning, G. Huyang, M. Ma, A. Beavis, D. Bishop, K. Cook, A. McDonagh, D. Shi, G.-D. Peng, M. Crossley, Percolation diffusion into self-assembled mesoporous silica microfibres, Nanomaterials 4 (2014) 157–174, https://doi.org/10.3390/nano4010157.
[80] G.L. Dotto, J.M.N. Santos, I.L. Rodrigues, R. Rosa, F.A. Pavan, E.C. Lima, Adsorption of Methylene Blue by ultrasonic surface modified chitin, J. Colloid Interface Sci. 446 (2015) 133–140, https://doi.org/10.1016/j.jcis.2015.01.046.
[81] F. Liu, L. Wang, D. Li, Q. Liu, B. Deng, A review: the effect of the microporous support during interfacial polymerization on the morphology and performances of a thin film composite membrane for liquid purification, RSC Adv. 9 (2019) 35417–35428, https://doi.org/10.1039/C9RA07114H.
[82] M. Dalwani, N.E. Benes, G. Bargeman, D. Stamatialis, M. Wessling, A method for characterizing membranes during nanofiltration at extreme pH, J. Membr. Sci. 363 (2010) 188–194, https://doi.org/10.1016/j.memsci.2010.07.025.
[83] G. Bargeman, J.M. Vollenbroek, J. Straatsma, C.G.P.H. Schroën, R.M. Boom, Nanofiltration of multi-component feeds. Interactions between neutral and charged components and their effect on retention, J. Membr. Sci. 247 (2005) 11–20, https://doi.org/10.1016/j.memsci.2004.05.022.
[84] J.-A.-D. Sharabati, S. Guclu, S. Erkoc-Ilter, D.Y. Koseoglu-Imer, S. Unal, Y. Z. Menceloglu, I. Ozturk, I. Koyuncu, Interfacially polymerized thin-film composite membranes: impact of support layer pore size on active layer polymerization and seawater desalination performance, Separ. Purif. Technol. 212 (2019) 438–448, https://doi.org/10.1016/j.seppur.2018.11.047.
[85] A.A. Yushkin, M.N. Efimov, A.O. Malakhov, G.P. Karpacheva, G. Bondarenko, L. Marbelia, I.F.J. Vankelecom, A.V. Volkov, Creation of highly stable porous polyacrylonitrile membranes using infrared heating, React. Funct. Polym. 158 (2021), 104793, https://doi.org/10.1016/j.reactfunctpolym.2020.104793.